Electronic Supplementary Material (ESI) for Soft Matter

Supplementary Information: Dispersions of ellipsoidal particles in a nematic liquid crystal

Mykola Tasinkevych,[1,2,*] Frédéric Mondiot,[3] Olivier Mondain-Monval,[3] and Jean-Christophe Loudet[3,†]

[1]*Max-Planck-Institut für Intelligente Systeme, Heisenbergstr. 3, D-70569 Stuttgart, Germany*

[2]*Institut für Theoretische Physik IV, Universität Stuttgart, Pfaffenwaldring 57, D-70569 Stuttgart, Germany*

[3]*Université Bordeaux 1, CNRS, Centre de Recherche Paul Pascal, Avenue A. Schweitzer F-33600 Pessac, France*

[*]Electronic address: miko@is.mpg.de

[†]Electronic address: loudet@crpp-bordeaux.cnrs.fr

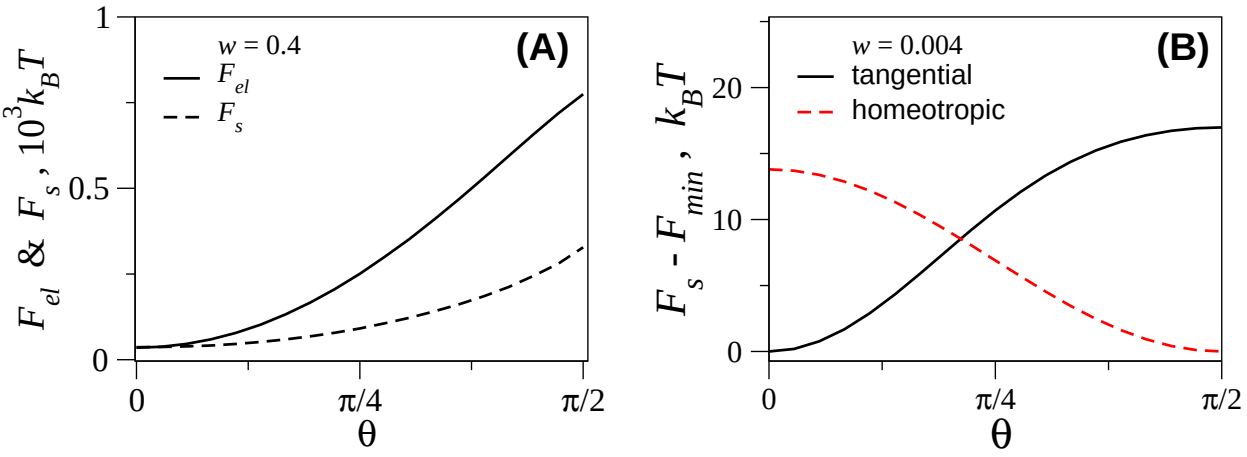

FIG. S1: **(A)** Elastic (F_{el}) and surface anchoring (F_s) contributions to the total free energy as a function of θ for weak tangential anchoring ($w = 0.4$) (see main text for details). **(B)** Ultra-weak tangential anchoring $w = 0.004$, $F_{el} \lesssim 10^{-8}$. Aspect ratio $k = 5$.

Supplementary Note 1
Weak and ultra-weak anchoring

Our main goal here is to provide additional information to explain the parabolic shape of the curves displayed on Fig. 4 of the main text.

Tangential anchoring. As mentioned in the main text, Brochard and de Gennes [54] predicted that, for a thin rod immersed in a nematic phase with *strong* non-degenerated tangential anchoring, the elastic free energy F_{el} scales as θ^2, where θ is the angle between the rod long axis and the far field director $\hat{\mathbf{n}}$. The experiments of Lapointe *et al.* confirmed this behavior [52]. The solid black line on Fig. 4 indicates that this θ^2 law seems to hold as well for weak degenerate anchoring ($w = 0.4$). The reason becomes clear if we analyse the contributions from the bulk elastic free energy F_{el} (the first integral in Eq. (1) minus the bulk free energy of a uniform nematic) and the surface anchoring free energy F_s (the second integral in Eq. (1)), which are both plotted in Fig. S1(A) as solid and dashed lines, respectively. We see that, even for $w = 0.4$, the bulk nematic distortions are still significant and F_{el} dominates F_s for all θ values (except at $\theta = 0$ where the two curves join). This result qualitatively explains the quadratic form of the solid black curve shown in Fig. 4.

Eventually, as the anchoring strength decreases even further, the bulk nematic distortions should fade away and the total free energy should be determined by the surface anchoring term only. Its contribution can be readily estimated within the Frank-Oseen model, where the surface free energy may be written in the form $F_s = \frac{W}{2}\int_{\partial\Omega}(\mathbf{n}\cdot\boldsymbol{\nu})^2 ds$. Here, $\boldsymbol{\nu}$ denotes the surface unit normal vector and $W > 0$ (resp. $W < 0$) describes a tangential (resp. homeotropic) anchoring. For $W \ll 1$, the far-field director $\hat{\mathbf{n}}$ is only slightly distorted by the presence of a colloidal particle. Assuming $\hat{\mathbf{n}}$ along the $z-$axis, the Frank-Oseen elastic free energy (in the one-elastic-constant approximation, K) may be approximated as [54]: $F_{el} \simeq \frac{K}{2}\int d^3r\,[(\nabla n_x)^2 + (\nabla n_y)^2]$, where $(n_x, n_y, 0)$ describes deviations of the local director from $\hat{\mathbf{n}}$. Consequently, for $n_{x,y} \ll 1$, the leading contribution, F_{lead}, to the free energy stems from the surface term, i.e., $F_{lead} = \frac{W}{2}\int_{\partial\Omega}(\nu_z)^2 ds$. We may approximate a large-k ellipsoid by a cylinder with radius R, then F_{lead} is readily integrated giving

$$F_{lead} = \pi W k R^2 \left(\sin^2\theta + \frac{\cos^2\theta}{k}\right), \tag{1}$$

where θ is the angle between the cylinder axis and $\hat{\mathbf{n}}$. For $k \to \infty$ (with $kR \to$ cst), the term $\frac{\cos^2\theta}{k}$, describing the cylinder ends effects, may be dropped yielding $F_{lead} \propto W \sin^2\theta$. Eq. (1) is valid for large θ too, and it agrees quite well with the numerical results displayed in Fig. S1(B), which are obtained for an ultra-weak anchoring strength ($w = 0.004$).

Homeotropic anchoring. It is rather surprising that a similar θ^2 behavior is also observed for the case of homeotropic anchoring, be it weak (see red dashed curve on Fig. 4) or strong (see open symbols around the global minima at $\theta = \pi/2$ on Figs. 2 & 3). We think that sharp deviations from the quadratic regime, reflected by the onset of a free energy barrier at small θ, and the rich free energy landscape are mainly caused by the interplay of the shape anisotropy and the topological defects induced by homeotropic boundary conditions.

Supplementary Note 2
Model parameters and the numerical procedure

As mentioned in the main text, we used the Landau-de Gennes theory to compute the total free energy related to the immersion of prolate ellipsoidal particles in a nematic phase. We here provide additional information about some variables defined in Eqs. (1)-(3) of the main text and outline the numerical procedure.

It is convenient to define the dimensionless temperature $\tau = 24ac/b^2$. At $\tau < 1$ the uniaxial nematic is stable and the degree of orientational order is given by

$$Q_b = \frac{b}{8c}\left(1 + \sqrt{1 - \frac{8\tau}{9}}\right). \tag{2}$$

The nematic becomes unstable at $\tau > 9/8$. At $\tau = 1$ both the nematic and the isotropic phases coexist. We use the following values of the model parameters: $a_0 = 0.044 \times 10^6$ J /Km^3, $b = 0.816 \times 10^6$ J/m^3, and $c = 0.45 \times 10^6$ J/m^3, $T^* = 307$ K, $L_1 = 6 \times 10^{-12}$J/m (these are typical values for 5CB [70]), and for simplicity we put $L_2 = 0$. The spatial extension of inhomogeneous regions and the cores of topological defects is of the order of the bulk correlation length, ξ, given by $\xi = \left(8c\left(3L_1 + 2L_2\right)/b^2\right)^{1/2} \simeq 10$nm at the nematic-isotropic (NI) transition [71]. The LdG elastic constants L_1 and L_2 may be related to the FO elastic constants, $K_1 = K_3$ and K_2, through the uniaxial ansatz $Q_{ij} = 3Q_b\left(n_i n_j - \delta_{ij}/3\right)/2$, yielding $K_1 = K_3 = 9Q_b^2(L_1 + L_2/2)/2$ and $K_2 = 9Q_b^2 L_1/2$ [72]. In general, K_1 and K_3

are different, but in most cases the difference is small and the LdG free energy is deemed adequate.

We minimize the Landau-de Gennes free energy (Eq. (1), main text) numerically by using adaptive finite elements methods. Initially, the surface of a colloidal particle is triangulated using Open Source GNU Triangulated Surface (GTS) library [73]. Then, the triangulation of the nematic domain Ω is carried out using *Quality Tetrahedral Mesh Generator* [74], which supports the adaptive mesh refinement. Linear triangular and tetrahedral elements are used in $2D$ and $3D$, respectively. Generalized Gaussian quadrature rules for multiple integrals [75] are used in order to evaluate integrals over elements. In particular, for tetrahedra a fully symmetric cubature rule with 11 points [76] is used, and integrations over triangles are done by using a fully symmetric quadrature rule with 7 points [77]. The discretized Landau-de Gennes functional in then minimized using the National Institute for Research in Computer Science and Control *M1QN3* [78] optimization routine, which implements a limited memory quasi-Newton technique of Nocedal [79]. More details on the numerical implementation can be found in ref. [80].

We only consider cylindrically symmetric ellipsoidal particles with semi-axes (A, B, B), where A (resp. B) is the semi-long (resp. semi-short) axis. Particles with aspect ratio $k \equiv \frac{A}{B} = 3, 5, 7$, and with a fixed volume $V = \frac{4}{3}\pi R_0^3$ are analyzed. In the single particle case, we use $R_0 = 0.3\,\mu$m. In the case of two ellipsoids, we study only the case $k = 5$, and set $B = 0.1\,\mu$m.

Supplementary References

[70] S. Kralj, S. Žumer, & D. W. Allender. Nematic-isotropic phase-transition in a liquid-crystal droplet. **43**, 2943-2954 *Phys. Rev. A* (1991).

[71] S. Chandrasekhar, *Liquid Crystals, 2nd ed.* (Cambridge University, 1992).

[72] F. C. Frank. On the theory of liquid crystals. *Disc. Faraday Soc.* **25**, 19-28 (1958).

[73] GNU Triangulated Surface Library, (2006). Available at http://gts.sourceforge.net.

[74] Si H. (2011) Tetgen: A Quality Tetrahedral Mesh Generator and a 3D Delaunay Triangulator.

Available at http://wias-berlin.de/software/tetgen/.

[75] R. Cools. An encyclopaedia of cubature formulas. *J. Complexity* **19**, 445-453 (2003).

[76] P. Keast. Moderate-degree tetrahedral quadrature-formulas. *Comput. Methods Appl. Mech. Eng.* **55**, 339-348 (1986).

[77] A. H. Stroud, Approximate calculation of multiple integrals (Prentice-Hall, Englewood Cliffs, N.J., 1971).

[78] Gilbert J. C. & Lemaréchal C. Some numerical experiments with variable storage quasi-Newton algorithms. *Mathematical Programming* **45**, 407-436 (1989). Available at https://who.rocq.inria.fr/Jean-Charles.Gilbert/modulopt/optimization-routines/m1qn3/m1qn3.html.

[79] J. Nocedal. Updating quasi-newton matrices with limited storage. *Math. Comput* **35**, 773-782 (1980).

[80] M. Tasinkevych, N. M. Silvestre & M. M. Telo da Gama. Liquid crystal boojum-colloids. *New J. Phys* **14**, 073030 (2012).